9th International Symposium on Hydraulic Structures Roorkee, India 24-27 October 2022
ISBN: 978-1-958416-07-5 DOI: https://doi.org/10.26077/9f7b-59e2

Near-full-scale physical modelling and open-channel flow velocity in a fish-friendly culvert with full-height sidewall baffles

J. Hu[1], Y. Li[1] & H. Chanson[1]
[1]*The University of Queensland, School of Civil Engineering, Brisbane, Australia*
E-mail: youkai.li@uq.edu.au

Abstract: *A near-full-scale physical modelling was performed on the oscillation and instability of open-channel flow in a fish-friendly culvert equipped with full-height sidewall baffles. High-resolution measurements of the instantaneous flow velocity were conducted using a Vectrino+ acoustic Doppler velocimeter (ADV). The physical results were marked by the existence of some low-frequency seiche phenomenon. A well-established triple decomposition technique was applied to the time series of free-surface and velocity time-series. The low-pass components confirmed a unique flow structure, consisting of a high-velocity zone in the main channel and a low-velocity flow reversal within the lateral cavities. The band-pass components corresponded to the low-frequency flow oscillations, highlighting the complicated transverse interactions between the lateral cavity and the main channel. The high-pass velocity components were related to the 'true' turbulence characteristics. The current study provides some further insights into the sustainable design of culverts to assist with upstream fish migration in man-made and natural fast waterways.*

Keywords: *Physical modelling; Sidewall baffle; Fish-friendly culvert; Hydrodynamics; Triple decomposition.*

1. Introduction

In eastern Australia, road crossings constitute a major hinderance for the upstream passage of small-body fish and juveniles of large fish, according to the Queensland and New South Wales Governments. These small individuals, less than 100 mm total length, have very limited swimming performance, typically with characteristic swimming speeds less than 0.3 m/s (Chanson and Leng 2021). Despite diverging opinions, a consensus suggests that the high-water velocities impact most adversely on the upstream passage of small-body weak-swimming fish (Pavlov et al. 1994, Chanson and Leng 2021). The installation of full-height sidewall baffles in standard box culverts is one of the proposed practical solutions to assist upstream passage for small-body fish species (Fig. 1). At low flow rates, the lateral baffles create a reduced flow velocity in the main flow as well as deliver rest areas in the lateral cavities, all of which assist upstream fish traversability (Duguay and Lacey 2014). Small-body fish and juveniles of large fish were observed to use the recirculation and stagnation zones, respectively behind and in front of sidewall baffles, to progress upstream and rest (Marsden 2015, Cabonce et al. 2018 and 2019). However, at larger flows, the full-height sidewall baffles were observed to drastically reduce the culvert conveyance and to cause hydrodynamic instabilities (Leng and Chanson 2020a).

The presence of lateral cavities in open channels leads to the formation of strong vortices in the separated shear zones, resulting in a range of water quality and ecological effects (Valentine and Wood 1979, Hill 2014). The hydrodynamic instabilities may be highly coherent when some coupling occurs between the separation layer and the natural wave modes in the channel and lateral cavity (Tuna et al. 2013, Perrot-Minot et al. 2020).Despite a wealth of research on subcritical flows past lateral cavities (Ohmoto et al. 2005, Yossef and De Vriend 2011), the study of flows past successive lateral cavities, including the interactions between cavities, has attracted a lesser interest, except a few studies (Meile et al. 2011, Tuna and Rockwell 2014, Leng and Chanson 2020b). Herein, new laboratory experiments were performed at the University of Queensland, in a relatively large and near-full-scale fish-friendly culvert model. The focus of the measurements was the free-surface instabilities and seiching, as well as the coupling between free-surface and velocity fluctuations.

2. Experimental setup and methods

2.1. Facility, instrumentation and flow conditions

The present laboratory experiments were conducted in a relatively-large-size facility acting at a near-full-scale box culvert barrel. The extrapolation of the results to larger prototype structures would be based upon a combined Froude

and Morton similitude, with a geometric scale from 1:1 to 1:4 corresponding to typical precast concrete boxes between 0.5 m and 2 m in width for culvert construction. The physical testing was performed in a 15 m long 0.5 m wide (B = 0.50 m) horizontal flume (Fig. 2). The invert of the flume was made of smooth PVC and the sidewalls were made of transparent tempered glass. The discharge was fed to the flume by a 2.0 m long 1.25 m wide intake basin, equipped with baffles, flow straighteners and three-dimensional convergent leading to the 0.5 m wide channel. The water was supplied by a constant head tank. The flume ended with a free overfall at the downstream end.

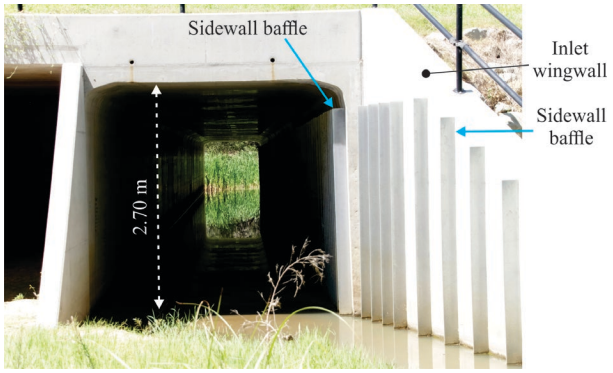

Figure 1. Multicell box culvert equipped with sidewall baffles in Flagstone QLD (Australia) on 2 October 2021 - Details of culvert inlet and barrel start, with sidewall baffles (baffle width: h_b = 0.150 m, cavity length: L_b = 0.60 m) installed to assist with upstream fish passage

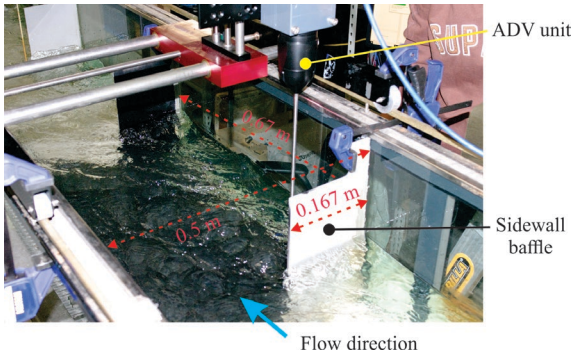

Figure 2. Experimental facility and instrumentation at the University of Queensland - Flow conditions: Q = 0.055 m^3/s, h_b =0.167 m, L_b = 0.67 m, flow direction from bottom right to top left as indicated by the blue arrow.

The channel was equipped with relatively large sidewall baffles (h_b = 0.167 m) placed on the right sidewall, with h_b the baffle size in the direction normal to the sidewall. The baffles were plain rectangular, and the longitudinal spacing interval was L_b = 0.67 m and 0.33 m. A constant baffle spacing was used for a given set of experiments. The baffles were fixed to the false floor and held at the top, and clay was used to seal the gaps between the baffles and sidewall.

The water discharge was measured with a Venturi meter placed on the pipeline of the water reticulation system. The meter was designed and built based upon British Standard (1943). The error of the discharge was less than 2%. The centreline water elevation was measured with a pointer gauge, with an accuracy of ±0.5 mm. Unsteady free-surface recordings were performed with two independent techniques: backlighting through the glass sidewalls and ultrasonic sensors mounted above the channel. In the former, two high-speed video cameras: Casio™ EX-10 at 120 fps and Sony™ RX100V at 100 fps were utilised. In the latter, a set of nine Microsonic™ Mic+25 ultrasonic acoustic displacement meters (ADMs) were sampled at 200 Hz.

The velocities were measured with a Nortek™ Vectrino+ acoustic Doppler velocimeter (ADV), equipped with a side-looking head. The ADV signal was sampled at 200 Hz for 180 s at each location. All ADV signal data were post-processed to remove erroneous data and spikes. Data with an average correlation of less than 60% and an average SNR less than 5 dB were removed, and the signal was "despiked" using a phase-space thresholding technique (Goring and Nikora 2002, Wahl 2003, Mori et al. 2007, Chanson et al. 2008).

2.2. Triple decomposition of free-surface and velocity data

Both water elevation and velocity data showed the presence of some seiching in the form of low-frequency oscillations with periods about 1 s to 3 s, depending upon the discharge and boundary conditions. A typical illustration is presented in Figure 3. A triple decomposition of the instantaneous water elevation and velocity component data was applied following earlier works in riverine systems (Hussian and Reynolds 1972, Fox et al. 2005, Brown and Chanson 2013). That is, the instantaneous time-series may be represented as a superposition of three components:

$$V = < V > + [V] + \{V\} \quad (1)$$

where V is the instantaneous measurement, <V> is the low-pass filtered contribution, [V] is the slow fluctuating component, or band-pass filtered, and {V} is the high-pass filtered component, corresponding to 'true' turbulence. A detailed sensitivity analysis was undertaken in terms of the selection of physically meaningful cutoff frequencies, f_1 and f_2. Herein, f_1 is the upper cutoff frequency of the low-pass filtered component, and f_2 is the lower cutoff frequency of the high-pass filtered signal. The results of the sensitivity analysis showed that the mean contribution <V> was little affected by a cut-off frequency $f_1 < 1/3 \times f_d$, with f_d the dominant frequency (Fig. 3), while the 'true' turbulent component {V} was nearly independent of an upper cut-off frequency $f_2 > 3 \times f_d$. Thus, the triple decomposition was applied to both water elevations and velocity components using: $f_1 = 1/3 \times f_d$ and $f_2 = 3 \times f_d$. Note that the ADV signal data were post-processed to remove erroneous data and spikes, before applying the triple decomposition analysis.

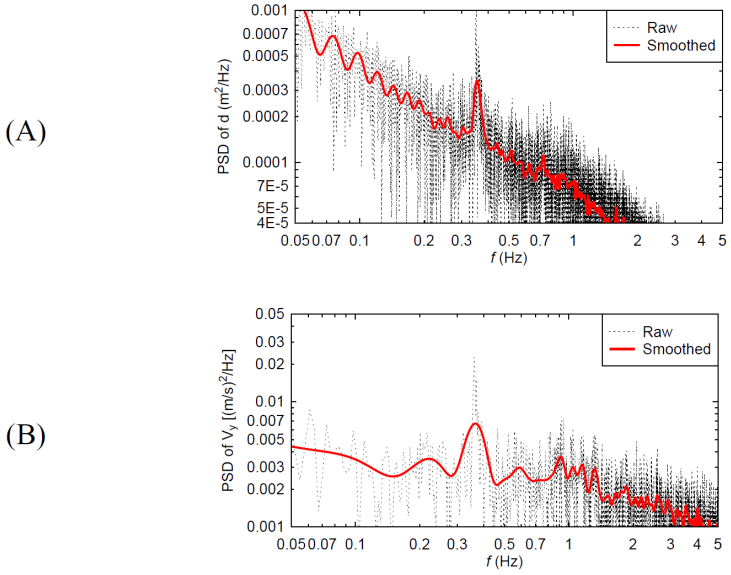

Figure 3. Fast Fourier transform (FFT) analyses of water elevation and transverse velocity signals: (A) Water elevation measured on the channel centreline at half-distance between two baffles $x\text{-}x_b = 0.335$ m, $y = 0.25$ m; (B) Transverse velocity component at $x\text{-}x_b = 0.335$ m, $y = 0.25$ m, $z = 0.0078$ m. – Herein, x is the longitudinal coordinate starting from the upstream end of the flume, y is the transverse coordinate starting from right sidewall, z is the vertical coordinate starting from the PVC false floor, $x_b = 8.20$ m indicates the longitudinal location of the upstream baffle of the test cavity.

3. Basic flow patterns

Visual, photographic and video observations were undertaken to record the basic open channel flow patterns for 0.029 $m^3/s < Q < 0.0925$ m^3/s with $L_b = 0.67$ m and for 0.029 $m^3/s < Q < 0.056$ m^3/s with $L_b = 0.33$ m. The observations were conducted about 6.2 m < x < 9 m, with x the longitudinal distance from the upstream end of the glass-walled channel.

The open channel flow passed beside the lateral cavities sequentially and presented a strong turbulent motion (Fig. 2). The main stream propagated downstream, while some recirculation was seen in the cavity regions between adjacent sidewall baffles. Some water stagnation occurred on the upstream side of the baffles, locally creating an increased

free-surface elevation at the upstream corner. Separation took place at the outer edge of each baffle, inducing cross-waves propagating downstream. Overall, the free-surface was very rough and unstable (Fig. 2). Large-scale turbulent structures and surface scars were seen through the whole channel. Dye injection revealed some complicated recirculation motion behind the baffles for the full cavity length between baffles. These were investigated more specifically using neutral-buoyancy particles (Li and Chanson 2020).

Free-surface waves and instabilities were observed for the full length of the channel, both in the main stream and in the lateral cavities (Fig. 4). The water depth constantly fluctuated with time, and relatively large wave heights were observed in both the mainstream and the cavities between baffles. The unstable water surface created some considerable amount of individual air bubble entrainment, especially at larger discharges. Based upon the non-intrusive instantaneous water recordings, the dominant frequency f_d of water surface oscillations was found to be identical in the main stream and lateral cavity. Typical results are reported in Table 1. For three flow conditions, the dominant frequency results were found to be identical for both water elevation and instantaneous velocity component data.

Furthermore, the mean wave height and maximum wave height were also documented, based on the ADM sampling over the centreline at the middle longitudinal location of the test cavity for 0.029 $m^3/s < Q < 0.0925$ m^3/s with L_b = 0.67 m. For increasing flow rates during the current experiments, both the mean wave height and maximum wave height increased. For each flow rate, the maximum wave height was about twice the value of the mean wave height. The maximum wave heights were approximately 20% of the mean water depths. The results are reported in Figure 5.

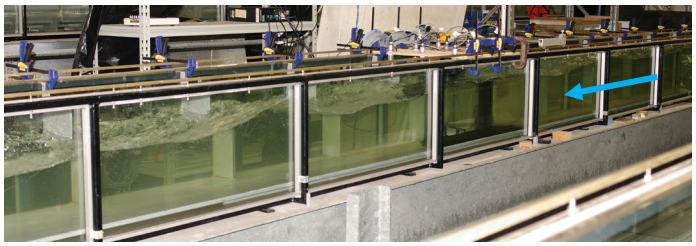

Figure 4. Sidewall baffled channel in operation for Q = 0.0925 m^3/s, h_b = 0.167 m, L_b = 0.667 m, S_o = 0 - Sideview through the (smooth) left sidewall, with flow direction from right to left as indicated by the arrow (shutter speed: 1/80 s)

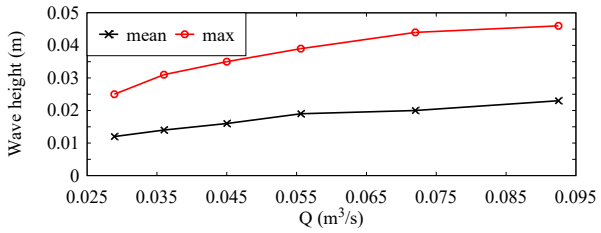

Figure 5. The average and maximum wave height from surface elevation measurements using ADM – Flow conditions: 0.029 $m^3/s < Q < 0.0925$ m^3/s, L_b = 0.67 m.

Table 1. Dominant frequencies f_d of instantaneous free-surface oscillations derived FFT analyses (for x_b = 8.20 m)

Q (m^3/s)	L_b (m)	h_b (m)	d_o (m)	V_o (m/s)	f_d (Hz) ([1])	Re	$f_d \times L_b/V_o$ ([1])
0.0289	0.33	0.167	0.125	0.46	0.83	1.54×10^5	0.59
0.0289	0.67	0.167	0.132	0.44	0.36	1.51×10^5	0.55
0.0360	0.67	0.167	0.156	0.46	0.38	1.77×10^5	0.55
0.0450	0.67	0.167	0.180	0.50	0.42	2.09×10^5	0.56
0.0556	0.33	0.167	0.192	0.58	0.47	2.51×10^5	0.27
0.0556	0.67	0.167	0.204	0.54	0.44	2.44×10^5	0.54
0.0720	0.67	0.167	0.245	0.59	0.47	2.90×10^5	0.53
0.0925	0.67	0.167	0.286	0.65	0.50	3.45×10^5	0.52

Notes: d_o: characteristic water depth in the main stream; Re: Reynolds number defined in terms of the hydraulic diameter; V_o: cross-sectional-averaged bulk velocity; ([1]) Dominant frequencies for instantaneous free-surface and/or velocity oscillations.

4. Velocity field

4.1. Mean velocity field

Velocity measurements were undertaken in the sidewall-baffled channel at three longitudinal locations and 7 or 10 transverse positions, with a minimum of 30 to 35 points per vertical profiles, leading to over 200 sampling points per cross-section at a specific longitudinal location, for a given flow condition. Herein, V_x is the longitudinal velocity component positive downstream, V_y is the transverse velocity component positive towards the left sidewall and V_z is the vertical velocity component positive upwards. Similarly, x is the longitudinal coordinate positive downstream with x = 0 at the upstream end of the glass-sidewalled channel, y is the transverse coordinate with y = 0 at the right sidewall and z is the vertical coordinate with z = 0 at the invert. The longitudinal location of upstream baffle of the test cavity is x_b.

The longitudinal velocity datasets presented a mean trend which was consistent with previous Prandtl-Pitot tube data obtained with a slightly different baffle configuration (h_b = 0.083 m, L_b = 0.333 m, Q = 0.054 m^3/s) (Leng and Chanson 2020b). The present data delivered a much greater level of details because of the high temporal resolution of the ADV system and its ability to measure instantaneous negative velocities. All the velocity data highlighted a major impact of the lateral baffles on the entire flow field, with some overall slower velocity and higher water depth, compared to a smooth (un-baffled) channel data. The presence of sidewall baffles modified the vertical profiles of longitudinal velocity component on the channel centreline (Fig. 6). While the centreline velocity data on a smooth (un-baffled) invert was characterised by a partially developed turbulent boundary layer flow with an ideal fluid flow region above (Leng and Chanson 2020b), the present centreline velocity distributions presented a velocity maximum at about z/d ~ 0.45, with a decreasing longitudinal velocity with increasing elevation for 0.45 < z/d < 1, in the baffled channel, with d the water depth. That is, the data showed a marked velocity dip next to the free surface. Moreover, negative velocities were recorded in the wake of the lateral baffle, i.e. $0 < z << h_b$.

Typical velocity contour maps are shown in Figure 7. The longitudinal velocity component data showed three distinctive regions: (1) a well-defined high-velocity flow region for $h_b << y < B$, (2) a shear zone with large transverse velocity gradient $\partial Vx/\partial y$ downstream of the baffle's outer edge ($y \sim h_b$) and (3) a recirculation region with negative longitudinal velocities for $0 < y << h_b$ (Fig. 7A). The time-averaged negative velocities reached values as low as -0.15 m/s. The transverse velocities showed magnitudes smaller than the longitudinal velocity components, and their contour maps implied some strong secondary currents, especially in the shear zone (Fig. 7B).

The velocity data were checked for the conservation of mass. The water discharge Q was compared to the integration of the time-averaged longitudinal velocity data assuming a no-slip condition at the invert and on both sidewalls:

$$Q = \iint_A V_x \times dy \times dz \tag{2}$$

with A the cross-section area of the flow. The results demonstrated the conservation of mass to be within less than 7% at all longitudinal locations. The time-averaged transverse velocity data were also integrated over the cross-section area to ensure the no-flow-through condition:

$$0 = \iint_A V_y \times dy \times dz \tag{3}$$

The results showed a reasonable agreement. For completeness, a continuity check could not be conducted meaningfully in terms of the vertical velocity component, because of the large water elevation oscillations.

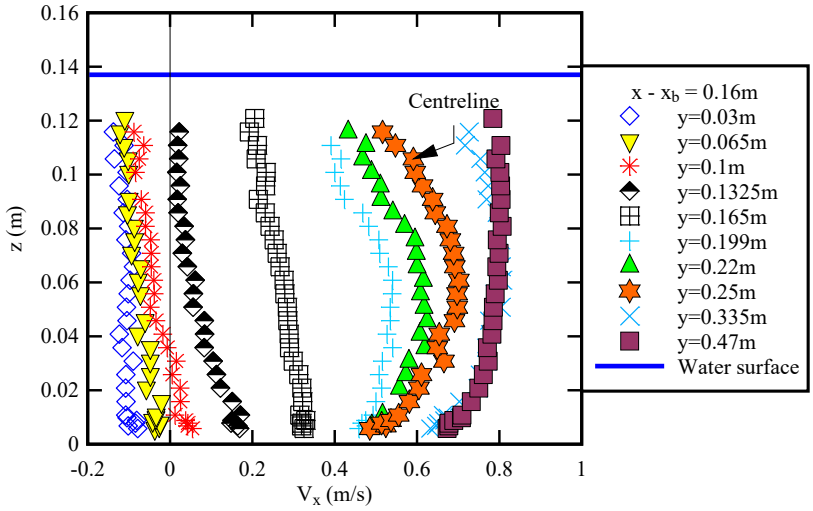

Figure 6. Vertical profiles of time-averaged longitudinal velocity for Q = 0.029 m^3/s, x_b = 8.2 m, h_b = 0.167 m, L_b = 0.667 m, $(x-x_b)/L_b$ = 0.25.

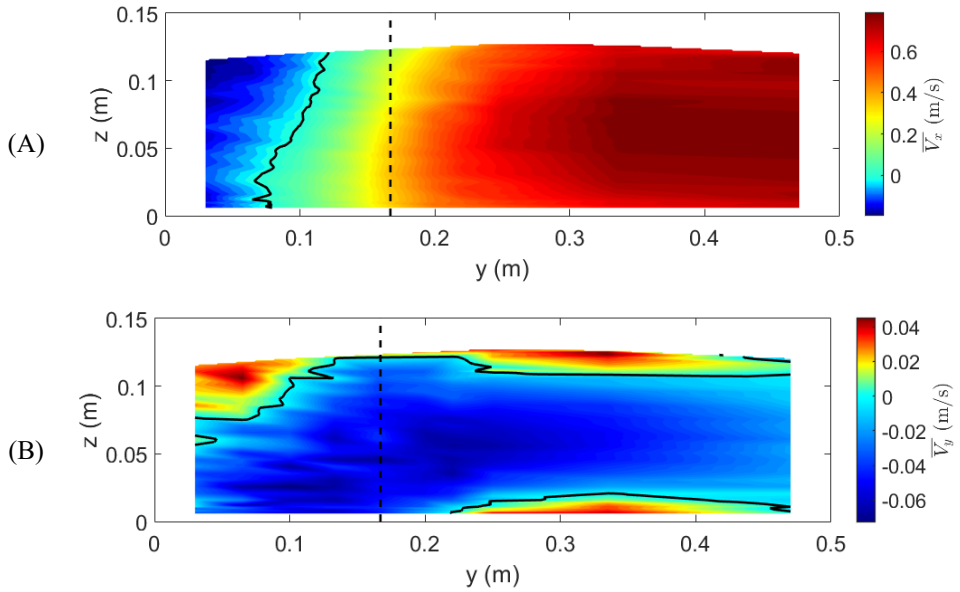

Figure 7. Contour maps of time-averaged longitudinal (A) and transverse (B) velocity components for Q = 0.029 m^3/s, x_b = 8.2 m, h_b = 0.167 m, L_b = 0.667 m, $(x-x_b)/L_b$ = 0.5 - The dashed black vertical line is the outer edge of the baffle; the solid black line corresponds to $\overline{V} = 0$.

4.2. Shear zone and recirculation

The flow between two baffles might be idealised as a two-dimensional supported jet, with a jet discharging from a nozzle of breadth (B - h_b) and expanding into a confined space with a total width B. Neglecting energy and momentum loss, the equations of conservation of mass and momentum imply between two baffles:

$$Q = \int_{y=0}^{B} \int_{z=0}^{d} V_x \times dz \times dy = \text{cons tan t} \tag{4a}$$

$$M = \int_{y=0}^{B} \int_{z=0}^{d} \rho \times V_x^{\,2} \times dz \times dy = cons\,tan\,t \tag{4b}$$

where Q is the water discharge and M the momentum flux. Some theoretical models of the flow in recirculation cavities were developed (Kimura and Hosoda 1997, Mizumura and Yamasaka 2020). Hill (2014) proposed a simplistic theoretical model of the recirculation velocity profile, associated with gyres and dead zones in river channels with lateral cavity. Assuming that the gyre diameter equals the baffle size h_b, and that the dimensionless interfacial shear along the cavity is approximately the dimensionless total drag, the predicted velocity distribution in the lateral cavity is presented in Fig. 8. Figure 8 compares further the theoretical model with the measured depth-averaged velocity. Although the gyre model was not developed for long lateral cavities, it showed a relatively close agreement with the data (Fig. 8).

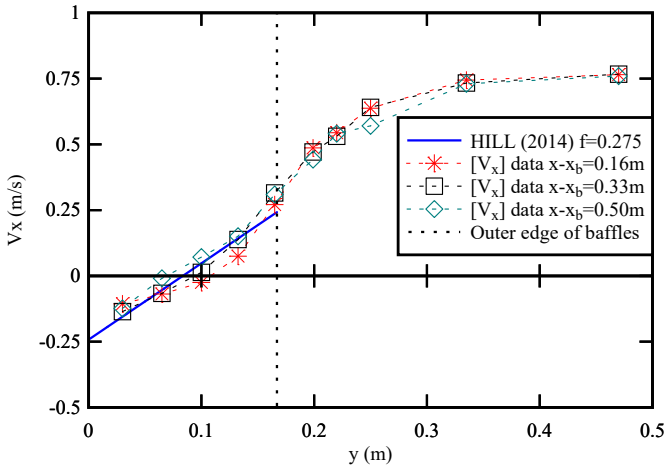

Figure 8. Transverse distribution of depth-averaged longitudinal velocity V_x in channel with sidewall baffles - Comparison with the theoretical model of cavity recirculation by Hill (2014) assuming f = 0.275 - The dashed black vertical line marks the outer edge of the sidewall baffle. – Flow conditions: Q = 0.029 m^3/s, x_b = 8.2 m, h_b = 0.167 m, L_b = 0.667 m

4.3. Velocity fluctuations

The flow was very turbulent in the sidewall-baffled channel. Large velocity fluctuations were observed in all three directions, with the largest fluctuations typically in the shear zone located in the wake of the outer edge of the baffle. Large turbulent intensities were recorded with V_x'/V_o up to 70%, V_y'/V_o up to 30% and V_z'/V_o up to 100%.

For each velocity measurement experiment, the three velocity components were recorded at three longitudinal cross-sections, and the triple-decomposition of the signals was applied to determine the contribution of the slow water surface oscillations on the turbulent fluctuations. For all the experiments, [V]' presented higher values on the right (baffle-side) half of channel. This was directly caused by the impact of the baffles. In contrast, the high velocity zone presented smaller [V]' values. Basically, the slow oscillations contributed more to turbulent fluctuations in the cavity and shear regions than in the main flow region. Typical data of velocity fluctuations [V]' induced by slow oscillations are shown in Figure 9. A dominant feature was that all data {V}' presented a higher value region in the shear zone (Fig. 10). There, i.e. in the wake of the outer edge of baffle, the transverse velocity data $\{V_y\}'$ always presented some significantly increased values in the shear zone because of the secondary currents associated with transverse momentum transfer (Fig. 10B). The transverse velocity data $\{V_z\}'$ showed high values in the near vicinity of the-free surface, as a direct consequence of free-surface unsteadiness. Figure 10 shows some 'true' turbulence generated by high-frequency velocity fluctuations. Overall, the standard deviations of the high-pass velocity components were the largest for the longitudinal and vertical components, with $\{V_x\}'/V_x' \sim 62\%$ to 77% in average and $\{V_z\}'/V_z' \sim 83\%$ to 90% in average. For the transverse velocity component, the contribution from band-pass and high-pass components were comparable: i.e., $[V_y]'/V_y' \sim \{V_y\}'/V_y'$. For comparison, the band-pass filtered fluctuations of the water elevation were the largest component with $[d]'/d' \sim 85\%$ in average.

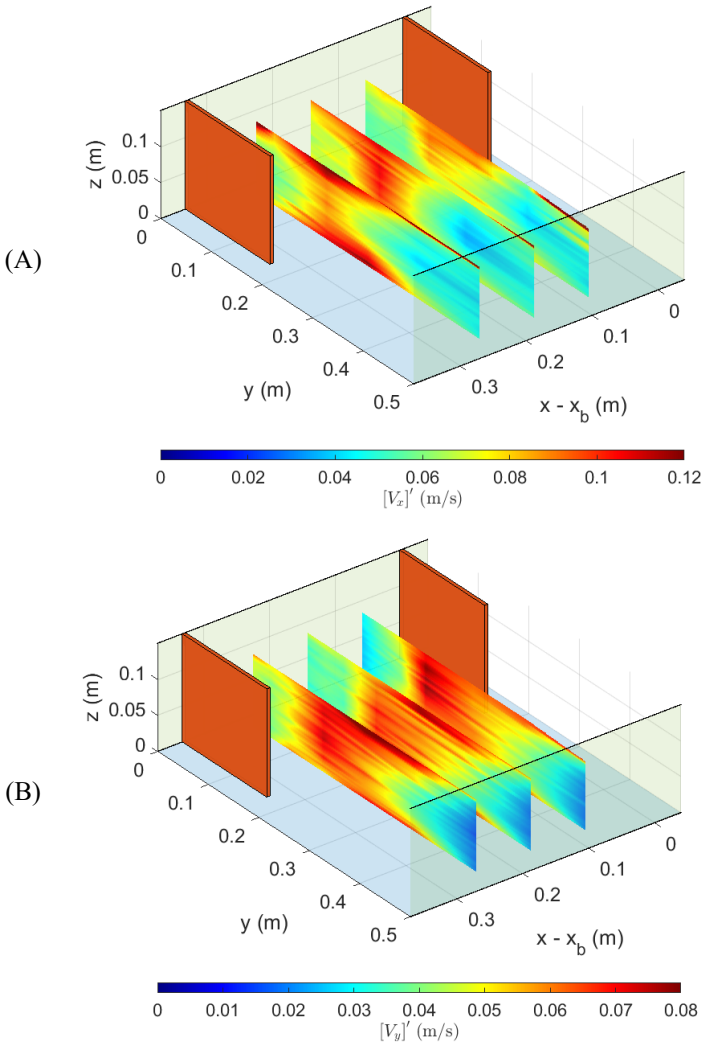

Figure 9. Standard deviation of band-pass filtered (0.3 -3.0 Hz) longitudinal (A)and transverse (B) velocity components for Q = 0.029 m^3/s, x_b = 8.2 m, h_b = 0.167 m, L_b = 0.333 m, d_o =0.125 m - Flow direction from top right to bottom left

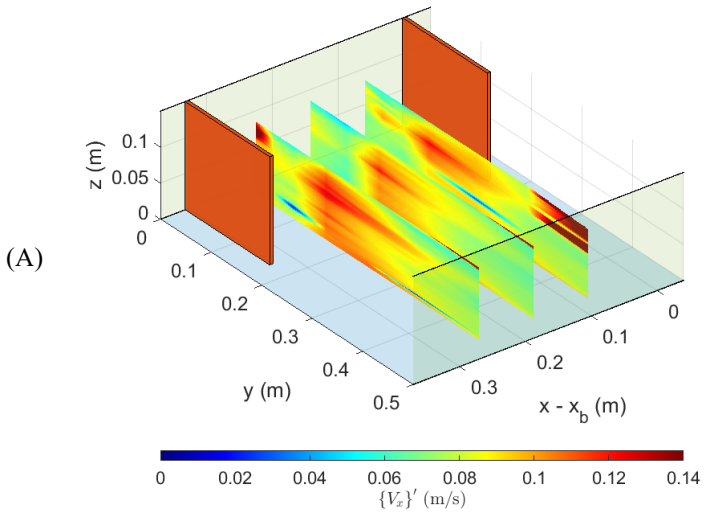

(B)

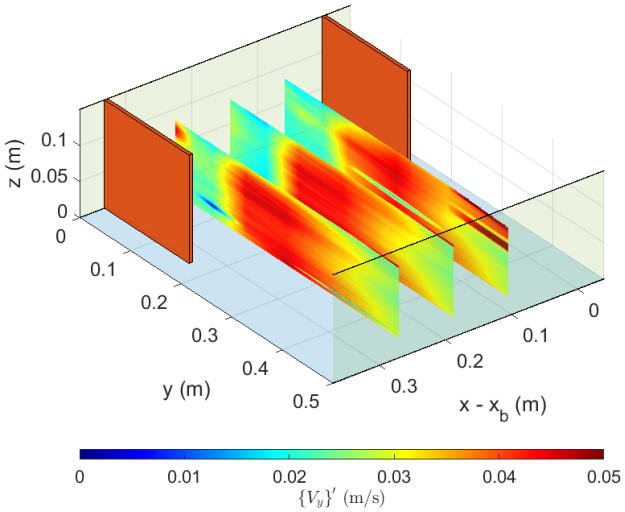

Figure 10. Standard deviation of high-pass filtered (3 -100 Hz) longitudinal (A)and transverse (B) velocity components for Q = 0.029 m^3/s, x_b = 8.2 m, h_b = 0.167 m, L_b = 0.333 m, d_o =0.125 m - Flow direction from top right to bottom left

5. Conclusion

Detailed instantaneous measurements of water surface elevation and velocity were recorded in a near-full-scale box culvert barrel equipped with sidewall baffles on one side. While the design was developed to assist upstream passage of small fish at low flows, the sidewall baffles induced strong hydrodynamic instabilities at medium to large discharges. These instabilities include relatively slow oscillations of the water surface in the entire channel, with maximum amplitude up to 20% of the average water depth, as well as oscillations of all three velocity components.

The mean velocity field showed a high velocity zone in the main stream besides the baffles, a recirculation zone behind the baffles with marked negative velocities, and a shear region in between characterised by intense secondary motion. The water depth and velocity signals were analysed using a triple decomposition approach, to quantify the impact of the slow oscillation on the velocity fluctuations. The slow oscillations were the major source of free-surface turbulence and turbulent velocity in the transverse direction. For the longitudinal and vertical velocity component, the high-frequency fluctuations were dominant.

In practical design applications, the impact of baffles encompasses an increased fish traversability at low flows and a greater total cost linked to the installation costs of baffles, the increase in the number of barrel cells to achieve the same design discharge and afflux, and operational maintenance. In practice, sediment and debris trapped by the baffles must be mitigated since these may drastically reduce the conveyance of flow and impede upstream fish passage. Besides, based on the communication with Queensland Fire and Emergency Services, the baffles, typically manufactured in steel, may also create a potential hazard to swift water rescue and emergency personnel during rescue operations. All the above problems need to be considered for both further research and prototype designs.

6. Acknowledgements

The authors thank Jason Van Der Gevel and Stewart Matthews (The University of Queensland) for their technical assistance.

7. References

British Standard (1943). "Flow Measurement." *British Standard Code BS 1042:1943*, British Standard Institution, London.

Brown, R, and Chanson, H. (2013). "Turbulence and Suspended Sediment Measurements in an Urban Environment during the Brisbane River Flood of January 2011." *Journal of Hydraulic Engineering*, Vol. 139, No. 2, pp. 244-252.

Cabonce, J., Wang, H., and Chanson, H. (2018). "Ventilated Corner Baffles to Assist Upstream Passage of Small - Bodied Fish in Box Culverts." *Journal of Irrigation and Drainage Engineering, ASCE,* Vol. 144, No. 8, Paper 0418020, 8 pages.

Chanson, H., and Leng, X. (2021). "Fish Swimming in Turbulent Waters. Hydraulics Guidelines to assist Upstream Fish Passage in Box Culverts." CRC Press, Leiden, The Netherlands, 202 pages and 19 video movies.

Chanson, H., Trevethan, M., and Aoki, S. (2008). "Acoustic Doppler Velocimetry (ADV) in Small Estuary: Field Experience and Signal Post-Processing." *Flow Measurement and Instrumentation*, Vol. 19, No. 5, pp. 307-313.

Duguay, J., and Lacey, R.W.J. (2014). "Effect of Fish Baffles on the Hydraulic Roughness of Slip-Lined Culverts." *Journal of Hydraulic Engineering*, ASCE, Vol. 141, No. 1, Paper 04014065, 10 pages.

Fox, J.F., Papanicolaou, A. N., and Kios, L. (2005). "Eddy taxonomy methodology around submerged barb obstacle within a fixed rough bed." *Journal of Engineering Mechanics*, ASCE, Vol. 131, No. 10, pp. 1082-1101.

Goring, D.G., and Nikora, V.I. (2002). "Despiking Acoustic Doppler Velocimeter Data." *Journal of Hydraulic Engineering*, ASCE, Vol. 128, No. 1, pp. 117-126.

Hill, D.F. (2014). "Simple Model for the Recirculation Velocity of Open-Channel Embayments." *Journal of Hydraulic Engineering*, ASCE, Vol. 140, No. 4, Paper 06014004, 5 pages.

Hussian, A.K.M.F., and Reynolds, W.C. (1972). "The Mechanics of an Organized Wave in Turbulent Shear Flow. Part2: Experimental Results." *Journal of Fluid Mechanics*, Vol. 54, Part 2, pp. 241-261.

Kimura, I., and Hosoda, T. (1997). "Fundamental Properties of Flows in Open Channels with Dead Zone." *Journal of Hydraulic Engineering*, ASCE, Vol. 123, No. 2, pp. 98-107.

Leng, X., and Chanson, H. (2020a). "How Full-Height Sidewall Baffles affect Box Culvert Capacity: Balancing Fish Passage and Discharge Requirements." *Australasian Journal of Water Resources,* Vol. 24, No. 2, pp. 248-256.

Leng, X., and Chanson, H. (2020b). "Asymmetrical Wall Baffles to Assist Upstream Fish Passage in Box Culvert: Physical Modeling." *Journal of Irrigation and Drainage Engineering*, Vol. 146, No. 12, Paper 04020037, 10 pages.

Li, Y., and Chanson, H. (2020). "Hydrodynamic Instabilities in Open-Channel Flow past Lateral Cavities." *Proceedings of 22nd Australasian Fluid Mechanics Conference AFMC2020*, Brisbane, Australia, 7-10 December.

Marsden, T. (2015). "Common Rail Proof of Concept and Baffle Field Trial Assessment Report." *Report to OceanWatch Australia*, Australasian Fish Passage Services, 26 pages.

Meile, T., Boillat, J.L., and Schleiss, A.J. (2011). "Water-surface oscillations in channels with axi-symmetric cavities." *Journal of Hydraulic Research*, IAHR, Vol. 49, No. 1, pp. 73-81.

Mizumura, K., and Yamasaka, M. (2002). "Flow in Open-Channel Embayment." *Journal of Hydraulic Engineering*, ASCE, Vol. 128, No. 12, pp. 1098-1101.

Mori, N., Suzuki, T., and Kakuno, S. (2007). “Noise of acoustic Doppler velocimeter data in bubbly flows.” *Journal of Engineering Mechanics*, ASCE, Vol. 133, No. 1, pp. 122-125.

Ohmoto, T., Hirakawa, R., and Watanabe, K. (2005). "Interaction between Water Surface Oscillations and Large Eddies in an Open Channel with Spur dikes." *Proc. 31th Biennial IAHR Congress*, Seoul, Korea.

Pavlov, D.S., LupandinN, A.I., and Skorobogatov, M.A. (1994). "Influence of Flow Turbulence on Critical Flow Velocity for Gudgeon (*Gobio gobio*)." *Doklady Biological Sciences*, Vol. 336, pp. 215-217.

Perrot-Minot, C., Mignot, E., Perkins, R., Lopez, D., and Riviere, N. (2020). "Vortex shedding frequency in open-channel lateral cavity." *Journal of Fluid Mechanics*, Vol. 892, A25, 11 pages.

Tuna, B.A., Tinar, E., and Rockwell, D. (2013). "Shallow flow past a cavity: globally coupled oscillations as a function of depth." *Experiments in Fluids*, Vol. 54, Paper 1586, 20 pages.

Tuna, B.A., and Rockwell, D. (2014). "Self-sustained oscillations of shallow flow past sequential cavities." *Journal of Fluid Mechanics*, Vol. 758, pp. 655-685.

Valentine, E.M., and Wood, I.R. (1979). "Experiments in Longitudinal Dispersion with Dead Zones." *Journal of Hydraulic Division*, ASCE, Vol. 105, No. HY9, pp. 999-1016.

Wahl, T.L. (2003). "Despiking Acoustic Doppler Velocimeter Data. Discussion." *Journal of Hydraulic Engineering*, ASCE, Vol. 129, No. 6, pp. 484-487.

Yossef, M.F.M., and De Vriend, H.J. (2011). "Flow Details near River Groynes: Experimental Investigation." *Journal of Hydraulic Engineering*, ASCE, Vol. 137, No. 5, pp. 504-517.

Oct 27th, 12:00 AM

Near-Full-Scale Physical Modelling and Open-Channel Flow Velocity in a Fish-Friendly Culvert with Full-Height Sidewall Baffles

J. Hu
The University of Queensland

Y. Li
The University of Queensland, youkai.li@uq.edu.au

H. Chanson
The University of Queensland